

Transport anisotropy of the pnictides studied via Monte Carlo simulations of a Spin-Fermion model

Shuhua Liang,^{1,2} Gonzalo Alvarez,³ Cengiz Şen,^{1,2} Adriana Moreo,^{1,2} and Elbio Dagotto^{1,2}

¹*Department of Physics and Astronomy, University of Tennessee, Knoxville, Tennessee 37996, USA*

²*Materials Science and Technology Division, Oak Ridge National Laboratory, Oak Ridge, Tennessee 37831, USA*

³*Computer Science and Mathematics Division and Center for Nanophase Materials Sciences, Oak Ridge National Laboratory, Oak Ridge, Tennessee 37831, USA*

(Dated: December 3, 2024)

An undoped three-orbital Spin-Fermion model for the Fe-based superconductors is studied via Monte Carlo techniques in two-dimensional clusters. At low temperatures, the magnetic and one-particle spectral properties are in agreement with neutron and photoemission experiments. Our main results are the resistance vs. temperature curves that display the same features observed in BaFe₂As₂ detwinned single crystals (under uniaxial stress), including a low-temperature anisotropy between the two directions followed by a peak at the magnetic ordering temperature, that qualitative appears related to short-range spin order and concomitant Fermi Surface orbital order.

PACS numbers:

Introduction. In early studies of Fe-based superconductors [1], it was widely assumed that Fermi Surface (FS) nesting was sufficient to understand the undoped-compounds magnetic order with wavevector $\mathbf{Q} = (\pi, 0)$ [2] and the pairing tendencies upon doping. Neutron scattering reports of spin-incommensurate order [3] are in fact compatible with the nesting scenario. However, several recent experimental results cannot be explained by FS nesting, including (i) electronic “nematic” tendencies in Ca(Fe_{1-x}Co_x)₂As₂ [4]; (ii) orbital-independent superconducting gaps [5] found using laser angle-resolved photoemission (ARPES) spectroscopy on BaFe₂(As_{0.65}P_{0.35})₂ and Ba_{0.6}K_{0.4}Fe₂As₂; and, more importantly for the investigations reported here, (iii) the report of local moments at room temperature (T) via Fe x-ray emission spectroscopy [6, 7]. Considering these experiments and others, a better location for the pnictides appears to be in the “middle” between the weak and strong Coulomb correlation limits [8–10]. Since an intermediate Hubbard U is difficult for most analytical approaches, there is considerable interest in the development of simple models and computational techniques that could provide insight into this difficult coupling regime. The Hartree-Fock (HF) approximation to the Hubbard model [11] cannot be applied at room T since HF approximations only lead to non-interacting fermions above the ordering temperature T_N , and the local moment physics [6] cannot be reproduced [12].

Recently, a Spin-Fermion (SF) model for the pnictides has been independently proposed by Lv *et al.* [13] and Yin *et al.* [14]. The model, very similar to those widely discussed for manganites, originally involved itinerant electrons in the xz and yz d -orbitals coupled, via an on-site Hund interaction, to local spins (assumed classical) that represent the magnetic moment of the rest of the Fe orbitals (considered localized). The Hund interaction is supplemented by a nearest-neighbor (NN) and next-NN

(NNN) classical Heisenberg spin-spin interaction. This SF model has interesting features that makes it suitable for the pnictides, particularly since by construction the model has itinerant electrons in interaction with local moments [6, 7] at all temperatures.

Phenomenological SF models have been proposed before for underdoped cuprates, with itinerant fermions representing carriers locally coupled to classical spins representing the antiferromagnetic order parameter. These investigations unveiled stripe tendencies [15], ARPES and optical conductivity results [16] similar to experiments, and even the dominance of the d -wave channel in pairing [17]. Thus, it is natural to apply now these ideas to the Fe superconductors.

As remarked already, SF models are also mathematically similar to models used for the manganites [18]. Then, all the experience accumulated in the study of Mn-oxides can be transferred to the analysis of SF models for Fe-superconductors. In particular, one of our main objectives is to study for the first time a SF model for pnictides employing Monte Carlo (MC) techniques, allowing for an unbiased analysis of its properties. Moreover, to test the model, a challenging experimental result will be addressed. It is known that for detwinned Ba(Fe_{1-x}Co_x)₂As₂ single crystals, a puzzling transport anisotropy has been discovered between the ferromagnetic (FM) and antiferromagnetic (AFM) directions [19]. In addition, the resistivity vs. T curves display a difficult to understand peak at $T_N \sim 130$ K, and the presumably weak effect of an applied uniaxial stress [19] still causes the anisotropy to persist well beyond T_N . However, recent neutron results suggest that the transport anisotropy may be actually caused by strain effects that cause a shift upwards of the tetragonal-orthorhombic and T_N transitions [20, 21], as opposed to an intrinsic rotational symmetry-breaking state not induced by magnetism or lattice effects. Then, theoretical guidance is

needed. While the low- T anisotropy can be explained as caused by the orbital-spin coupling in the $\mathbf{Q}=(\pi,0)$ state [22], the full transport curves at finite T define a challenge for SF models that will be here addressed for the nontrivial undoped case.

Model and Method. The SF model [13, 14] is given by

$$H_{\text{SF}} = H_{\text{Hopp}} + H_{\text{Hund}} + H_{\text{Heis}}. \quad (1)$$

The first term H_{Hopp} describes the Fe-Fe hopping of itinerant electrons. To better reproduce the band structure physics of pnictides [1], three orbitals (xz , yz , xy) will be used instead of two. The full expression for H_{Hopp} is cumbersome to reproduce here, but it is sufficient for the readers to consult Eqs.(1-3) and Table I of Ref. 23 for the mathematical form and the actual values of the hoppings in eV's. The density of relevance used here is $n=4/3$ [23]. The Hund interaction is simply $H_{\text{Hund}} = -J_{\text{H}} \sum_{i\alpha} \mathbf{S}_i \cdot \mathbf{s}^\alpha_i$, with \mathbf{S}_i the classical spin at site i ($|\mathbf{S}_i|=1$), and \mathbf{s}^α_i the itinerant-fermion spin of orbital α . The last term H_{Heis} contains the spin-spin interaction among the localized spins $H_{\text{Heis}} = J_{\text{NN}} \sum_{\langle ij \rangle} \mathbf{S}_i \cdot \mathbf{S}_j + J_{\text{NNN}} \sum_{\langle\langle im \rangle\rangle} \mathbf{S}_i \cdot \mathbf{S}_m$, where $\langle \rangle$ ($\langle\langle \rangle\rangle$) denote NN (NNN) couplings. $J_{\text{NNN}}/J_{\text{NN}}=2/3$ in all the results below, leading to $(\pi,0)/(0,\pi)$ magnetism [24].

The well-known Monte Carlo (MC) technique for SF-like models [18] will be here used to study H_{SF} at any T . In this technique, the actual acceptance-rejection MC steps are carried out in the classical spins, while at each step a full diagonalization of the fermionic sector (hopping plus on-site Hund terms) for fixed classical spins is performed via library subroutines in order to calculate the energy of that spin configuration. These frequent diagonalizations render the technique CPU-time demanding. The simulation is run on a finite 8×8 cluster with periodic boundary conditions (PBC) and uses the full H_{SF} model for the MC time evolution and generation of equilibrated configurations for the classical spins at a fixed T [25]. However, for the MC measurements those equilibrated configurations are assumed replicated in space but differing by a phase factor such that a better resolution is reached with regards to the momentum \mathbf{k} . Since a larger lattice with more eigenstates gives a more continuous distribution of eigenenergies, the procedure then reduces finite-size effects in the measurements. This well-known method is often referred to as ‘‘Twisted’’ Boundary Conditions (TBC) [26]. In practice, phases Φ are added to the hopping amplitudes, schematically denoted as ‘‘ t ’’, at the boundary via $t_{\text{TBC}} = e^{i\Phi} t$, with $\Phi = 2\pi m/M$ ($m=0,1,\dots,M-1$) such that the number of possible momenta in the x or y directions becomes $L=8 \times M$.

Results. Figure 1(a) contains the structure factor of the classical spins, defined as $S(\mathbf{q}) = \frac{1}{N^2} \sum_{i,j} \langle \mathbf{S}_i \cdot \mathbf{S}_j \rangle e^{i\mathbf{q} \cdot (\mathbf{i}-\mathbf{j})}$ (N = number of sites), illustrating the development of $\mathbf{Q}=(\pi,0)$ magnetic order as T is reduced. Since a ratio $J_{\text{NNN}}/J_{\text{NN}} > 1/2$ is ‘‘frustrating’’, finding \mathbf{Q} -order at $J_{\text{H}}=0$ is not surprising, but

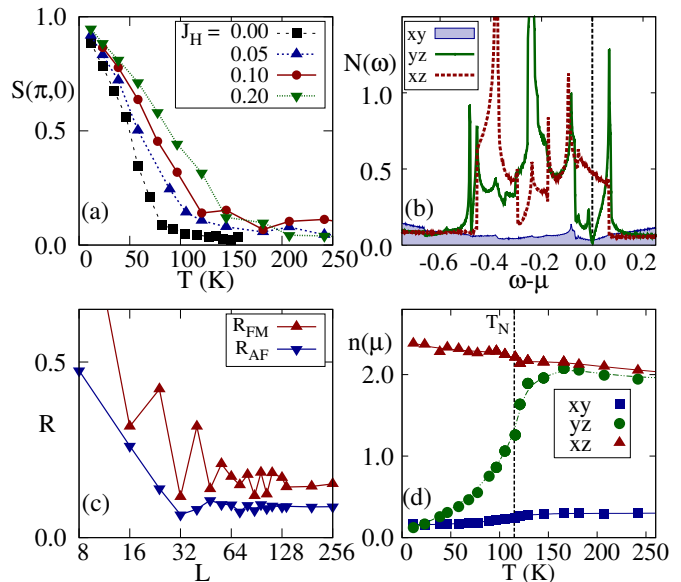


FIG. 1: (color online) (a) Classical spins structure factor $S(\pi,0)$ (normalized to 1) vs. T , for the J_{H} 's indicated, using the PBC 8×8 cluster and $J_{\text{NN}}=0.015$. The oscillations in the data are indicative of the error bars. (b) Density of states $N(\omega)$ of each orbital (μ = chemical potential), using TBC with $L=512$, at $T=0$ K and $J_{\text{H}}=0.1$ eV, for the perfect $(\pi,0)$ magnetic state. (c) Resistance R vs. L (TBC 8×8) for the FM and AFM directions of the perfect $(\pi,0)$ magnetic state ($J_{\text{H}}=0.1$ eV). (d) The occupation at the FS $n(\mu)$ (see text) of the three orbitals vs. T , using $L=256$. An asymmetry $J_{\text{NN}}=0.016$ (0.014) along the x (y) axis was used (see text).

Fig. 1 shows that this order remains stable turning on J_{H} in the range investigated, as opposed to inducing transitions to other states. The chosen value of J_{NN} in Fig. 1(a) leads to a T_{N} similar to that in BaFe_2As_2 . The low- T orbitally-resolved electronic density-of-states (DOS) is in Fig. 1(b). The \mathbf{Q} magnetic order opens a pseudogap (PG) in the yz orbital, while the others are not much affected. This PG generation was previously discussed when contrasting theory and ARPES experiments [27] and it should not be confused with long-range orbital-order, that in this SF model occurs at $J_{\text{H}} \sim 0.4$ or larger.

Figure 1(c) contains the evolution of the 8×8 -cluster resistance R increasing the number of momenta via the TBC, calculated via standard procedures [18, 28]. While the ratio of R 's along the FM and AFM directions is always > 1 , i.e. qualitatively correct, TBC with $L=256$ is needed to reach stable values. The occupation of the three orbitals at the FS (Fig. 1(d)) was defined as $n(\mu) = \int \text{den}(\epsilon) \beta e^{\beta(\epsilon-\mu)} / (1 + e^{\beta(\epsilon-\mu)})^2$, involving the μ -derivative of the fermionic population. As T increases and the \mathbf{Q} order weakens, the xz - yz orbitals populations converge to the same values.

The results of Fig. 1, and others below, were obtained introducing a ‘‘small’’ explicit asymmetry along the x and y axes for J_{NN} , namely a generalized J_{NN}^α ($\alpha=x,y$) was used. Its purpose is to mimic the orthorhombic distortion and strain effects [2] and judge if the present calcula-

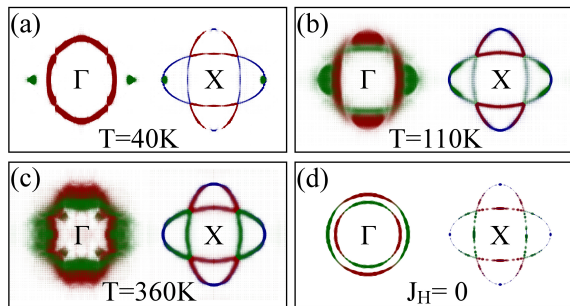


FIG. 2: (color online) $A(\mathbf{k}, \omega)$ at μ (TBC 8×8 $L=512$). (a-c) are for $J_H=0.1$ eV. Red, green, and blue are for the xz , yz , and xy orbitals, respectively. (a) $T=40$ K, below T_N . The $(\pi, 0)$ magnetic order induces yz -orbital electron satellite pockets. (b) $T=110$ K, i.e. at $\sim T_N$. In this regime, the MC configurations display small coexisting patches of $(\pi, 0)$ and $(0, \pi)$ order (see text), creating \sim -symmetric xz and yz features around Γ . (c) Large $T=360$ K, with no remnants of the $(\pi, 0)$ order. The FS is now a broadened version of the non-interacting one at $J_H=0$, shown in (d) at $T=100$ K.

tions reproduce transport experiments [19–21]. Consider the ratio $r_{NN}=J_{NN}^x/J_{NN}^y$. Using the well-known dependence of the hopping amplitudes with the distance u between d - and p -orbital active atoms i.e. $t_{pd} \sim 1/u^{7/2}$ [29], and fourth-order perturbation in the hoppings to evaluate the Fe-Fe superexchange leads to a crude estimation $r_{NN} \sim (a/b)^{20} \sim 1.07$ when the lattice parameters in Ref. 2 are employed. This is similar to the value used in the MC simulation $r_{NN} \sim 1.14$. Other crude estimations using formulas for the direct Fe-Fe hoppings [29] or employing the lattice parameters under pressure [20] lead to similar ratios. Then, our asymmetry is qualitatively realistic.

Previous investigations [11] showed that the $T=0$ HF approximation to the undoped multiorbital Hubbard model can reproduce neutron diffraction results and ARPES data. A similar degree of accuracy should be expected from any reasonable model for the pnictides, including H_{SF} . To test this assumption, the one-particle spectral function $A(\mathbf{k}, \omega)$ was calculated, and the FS at different T 's is shown in Fig. 2, contrasted against the low- T fermionic non-interacting limit $J_H=0$. At low- T in the ordered state the expected asymmetry between the $(\pi, 0)$ and $(0, \pi)$ electron pockets is observed (not shown), and more importantly satellite pockets (with electron character) develop close to the Γ hole pockets (Fig. 2(a)), as in ARPES experiments [11, 30]. Thus, the SF model studied here passes the low- T ARPES test. As T increases, at or well above T_N (Figs. 2(b) and (c)) the differences between the xz and yz are reduced and rotational invariance is recovered, albeit with a FS broader than in the non-interacting low- T limit (Fig. 2(d)).

R vs. T curves. Our most important results are the T dependence of R along the two axes, shown in Fig. 3. It is visually clear that these results are similar to the transport data of Ref. 19, particularly after realizing that phononic effects, that cause the continuous raise of R

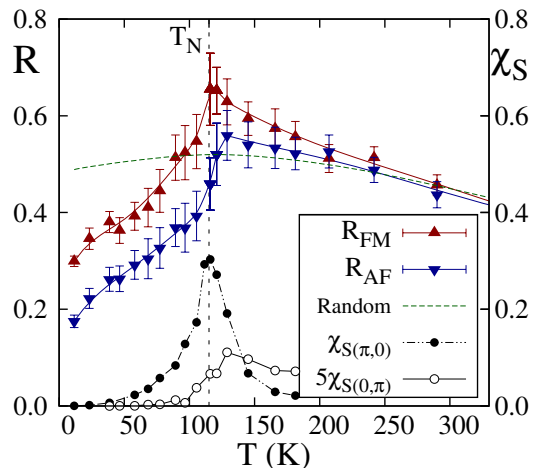


FIG. 3: (color online) Resistance R of the SF model calculated via MC simulations, at $J_H=0.1$ eV and using the $L=256$ TBC 8×8 cluster. T_N is indicated, together with magnetic susceptibilities χ_S . The asymmetry between the FM and AFM directions is evident at low T (note that the FM and AFM labels simply refer to the y and x directions, respectively, and not to fully FM or AFM spin configurations). As T increases the symmetry is restored, and the curves display a peak at T_N (see text). A small symmetry-breaking difference $r_{NN}=1.14$ is used (see text). In green are the results for random spin configurations, showing that their R is smaller than in the MC results near T_N . The width of the χ peaks extend to $\sim 1.5T_N$, in agreement with neutron scattering for CaFe_2As_2 [31].

with T in the experiments, are not incorporated in the SF model. At low T , a clear difference exists between the FM and AFM directions, induced by the $(\pi, 0)$ magnetic order that breaks spontaneously rotational invariance. At low- T this difference was understood in the Hubbard-model HF approximation [22] based on the reduction of the yz orbital population (Fig. 1(d)). This explanation is equally valid in the SF model, and at low T the SF model and the Hubbard model, when treated via the HF approximation, lead to similar physics.

The most interesting result in Fig. 3 is the development of a clear peak at T_N , and the subsequent slow reduction toward similar values along the FM and AFM directions with further increasing T (note that to model better the effect of uniaxial stress [19], a weak symmetry-breaking difference between the NN Heisenberg couplings along x and y was included, as already discussed). To our knowledge, this is the first time that the full R vs. T curve is successfully reproduced via a computational calculation, and the origin of these features will be discussed below.

A study as in Fig. 3 using a larger cluster, e.g. 16×16 , is not practical since the computer time grows like N^4 (N =number of sites), leading to an effort 256 times larger. However, results as in Fig. 1(a) indicate that the classical spins generated merely by the spin-spin interaction should be qualitatively similar to those generated by the full SF model, as long as J_H does not push the system into a new phase. Thus, the MC-time evolution

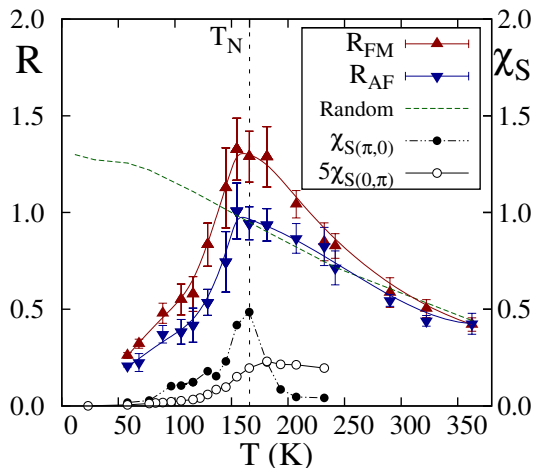


FIG. 4: (color online) Resistance R calculated using a $L=64$ TBC 16×16 cluster, with $J_{\text{NN}}=0.032$ (0.028) along the x (y) axis. The spin configurations are generated via H_{Heis} , while the R measurements use H_{SF} , at $J_{\text{H}}=0.1$ eV. The rest of the notation is as in Fig. 3.

could be carried out with H_{Heis} only, while measurements can still be carried out via a full diagonalization of H_{SF} . Those measurements (which are very CPU time consuming) need to be sufficiently sparsified in MC time to render the process practical. This procedure was implemented on a TBC 16×16 cluster, with $L=64$ [32]. The results for R are in Fig. 4, showing a remarkable qualitative similarity with Fig. 3, and with experiments. Thus, the essence of the R vs. T curves can be captured by electrons moving in the spin configurations generated by H_{Heis} . Size effects are small in the range analyzed here.

What causes the increase of R upon cooling before T_{N} , displaying insulating characteristics? Since our results have similar features as in experiments, an analysis of the MC-equilibrated configurations may provide a crude insight into their origin. In Fig. 5(a), a typical MC classical spins configuration is shown. The pattern of colors at the links illustrates the relative orientation of the two spins at the ends. The $(\pi, 0)$ long-range order is lost, but individual spins are not randomly oriented since the state contains small regions resembling locally either a $(\pi, 0)$ or $(0, \pi)$ order (short-range spin order). In fact, $S(\mathbf{q})$ still displays broad peaks at those two wavevectors. In standard mean-field approximations there are no precursors of the magnetic order above T_{N} , but in the SF model there are short-range fluctuations in the same regime.

States with “spin patches” as in Fig. 5(a) lead to a concomitant patchy orbital order at the FS, Fig. 5(b), where the two most populated orbitals at μ , xz and yz , are highlighted at every site. The orbital orientation shows that the xz (yz) FS population favors transport along the x (y) axis. The patchy order should have a resistance *larger* than that of a randomly-oriented spin background, as numerically confirmed by calculating R vs. T in the absence of a guiding Hamiltonian, i.e. by generating ran-

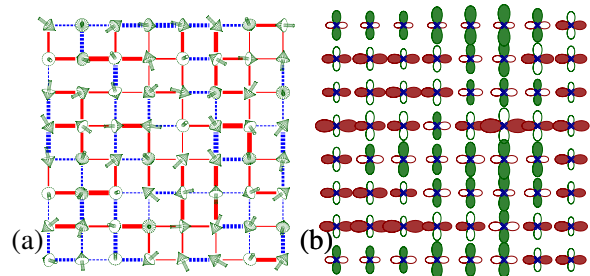


FIG. 5: (color online) (a) Typical MC-generated classical spin configuration on an 8×8 cluster at $T_{\text{N}} \sim 110$ K, $J_{\text{H}}=0.1$ eV, and $J_{\text{NN}}=0.016$ (0.014) along the x (y) axis. The red (blue) lines denote AFM (FM) NN correlations, of intensity proportional to the width. (b) The FS dominant orbital at each site for the configuration used in (a), calculated using $n(\mu)$ as in Fig. 1(d). Red (green) denote the xz (yz) orbital, with a size proportional to the density.

dom spin configurations. The results are in Figs. 3 and 4 (green dots) and, as expected, their values are *below* those of the peak resistance at T_{N} obtained with the full SF model, i.e. with configurations as in Fig. 5. Then, the strain coupled to short-range spin and FS orbital order appears related to the peak in the R vs. T curves [33]. Of course, this is merely a qualitative argumentation that can only be substantiated by detailed transport calculations involving, e.g., scattering rates. Reducing the small anisotropy used to mimic uniaxial stress the R - T curves display a concomitantly smaller anisotropy, but still have a small peak at T_{N} (not shown). Thus, the patchy states may also explain the insulating properties of $\text{Fe}_{1.05}\text{Te}$ [34] and $(\text{Tl,K})\text{Fe}_{2-x}\text{Se}_2$ [35] above T_{N} .

Conclusions. The Spin-Fermion model for pnictides was here studied with MC techniques. The magnetic and ARPES properties of the undoped pnictides are well reproduced. Including a small symmetry breaking to account for strain effects, the resistance R vs. T curves are qualitatively similar to those observed for BaFe_2As_2 [19], including a peak at T_{N} that appears caused by short-range spin and FS orbital order. In our calculations, the anisotropy above T_{N} exists as long as a strain distortion exists, compatible with results for annealed BaFe_2As_2 samples [36]. This successful application of a SF model paves the way to more demanding efforts involving doped systems at finite T where anisotropy effects are stronger than in the undoped limit [19].

Acknowledgment. The authors thank I.R. Fisher, M. Daghofer, S. Dong, W. Lv, S. Wilson, X. Zhang, Q. Luo, and A. Nicholson for useful discussions. This work was supported by the US Department of Energy, Office of Basic Energy Sciences, Materials Sciences and Engineering Division (S.L., C.S., A.M., E.D.). G.A. was supported by the Center for Nanophase Materials Sciences, sponsored by the Scientific User Facilities Division, BES, U.S. DOE. This research used resources of the National Center for Computational Sciences, as well as the OIC at ORNL.

-
- [1] D. C. Johnston, *Adv. Phys.* **59**, 803 (2010).
- [2] C. de la Cruz *et al.*, *Nature (London)* **453**, 899 (2008).
- [3] D. K. Pratt *et al.*, *Phys. Rev. Lett.* **106**, 257001 (2011).
- [4] T.-M. Chuang *et al.*, *Science* **327**, 181 (2010).
- [5] T. Shimojima *et al.*, *Science* **332**, 564 (2011).
- [6] H. Gretarsson *et al.*, *Phys. Rev. B* **84**, 100509(R) (2011).
- [7] F. Bondino *et al.*, *Phys. Rev. Lett.* **101**, 267001 (2008).
- [8] M. M. Qazilbash *et al.*, *Nat. Phys.* **5**, 647 (2009).
- [9] R. Yu *et al.*, *Phys. Rev. B* **79**, 104510 (2009).
- [10] Z.P. Yin, K. Haule, and G. Kotliar, *Nat. Mat.* **10**, 932 (2011).
- [11] Q. Luo *et al.*, *Phys. Rev. B* **82**, 104508 (2010).
- [12] Determinantal MC cannot be applied to the multiorbital case due to the “sign problem” even in the undoped limit.
- [13] W. Lv, F. Krüger, and P. Phillips, *Phys. Rev. B* **82**, 045125 (2010).
- [14] W.-G. Yin, C.-C. Lee, and W. Ku, *Phys. Rev. Lett.* **105**, 107004 (2010).
- [15] C. Buhler, S. Yunoki, and A. Moreo, *Phys. Rev. Lett.* **84**, 2690, (2000).
- [16] M. Moraghebi *et al.*, *Phys. Rev. B* **63**, 214513 (2001); M. Moraghebi *et al.*, *ibid* **66**, 214522 (2002).
- [17] M. Moraghebi, S. Yunoki, and A. Moreo, *Phys. Rev. Lett.* **88**, 187001 (2002).
- [18] E. Dagotto *et al.*, *Phys. Rep.* **344**, 1 (2001).
- [19] J.-H. Chu *et al.*, *Science* **13**, 824 (2010). See also I.R. Fisher, L. Degiorgi, and Z.X. Shen, *Rep. Prog. Phys.* **74**, 124506 (2011).
- [20] C. Dhital *et al.*, arXiv:1111.2326, to appear in PRL.
- [21] E. C. Blomberg *et al.*, arXiv:1111.0997.
- [22] X. Zhang and E. Dagotto, *Phys. Rev. B* **84**, 132505 (2011).
- [23] M. Daghofer *et al.*, *Phys. Rev. B* **81**, 014511 (2010).
- [24] The transition from (π, π) order to $(\pi, 0)/(0, \pi)$ order occurs at $J_{\text{NNN}}/J_{\text{NN}}=1/2$, within H_{Heis} .
- [25] Typically 20,000 MC sweeps through the lattice are performed for thermalization followed by 10,000 in equilibrium, with measurements every 20 configurations.
- [26] J. Salafranca *et al.*, *Phys. Rev. B* **80**, 155133 (2009).
- [27] M. Daghofer *et al.*, *Phys. Rev. B* **81**, 180514(R) (2010).
- [28] J. A. Vergés, *Comput. Phys. Commun.* **118**, 71 (1999).
- [29] W.A. Harrison, *Electronic Structure and the Properties of Solids*, (Dover, 1989).
- [30] M. Yi *et al.*, *Phys. Rev. B* **80**, 174510 (2009).
- [31] S.O. Diallo *et al.*, *Phys. Rev. B* **81**, 214407 (2010).
- [32] $\sim 200,000$ ($\sim 100,000$) MC steps for thermalization (measurements) were employed. The R calculations are very CPU time consuming, thus only ~ 20 were performed, but self-averaging effects render the error bars small.
- [33] The resistivity anisotropy has also been recently explained in similar terms via a nematic phase above T_{N} (R.M. Fernandes, E. Abrahams, and J. Schmalian, *Phys. Rev. Lett.* **107**, 217002 (2011)). The existence of a nematic phase in the SF model will be studied in the future.
- [34] G. F. Chen *et al.*, *Phys. Rev. B* **79**, 140509(R) (2009).
- [35] M. H. Fang *et al.*, *EPL* **94**, 27009 (2011).
- [36] M. Nakajima *et al.*, *PNAS* **108**, 12238 (2011).